Article

Fully Transparent and Highly Sensitive pH Sensor Based on an a-IGZO Thin-Film Transistor with Coplanar Dual-Gate on Flexible Polyimide Substrates

Tae-Hwan Hyun [ID] **and Won-Ju Cho** *[ID]

Department of Electronic Materials Engineering, Kwangwoon University, Seoul 139-701, Republic of Korea
* Correspondence: chowj@kw.ac.kr; Tel.: +82-2-940-5163

Abstract: In this paper, we propose a fully transparent and flexible high-performance pH sensor based on an amorphous indium gallium zinc oxide (a-IGZO) thin-film transistor (TFT) transducer with a coplanar dual-gate structure on polyimide substrates. The proposed pH sensor system features a transducer unit consisting of a floating gate (FG), sensing gate (SG), and control gate (CG) on a polyimide (PI), and an extended gate (EG) sensing unit on a separate glass substrate. We designed a capacitive coupling between (SG) and (CG) through the FG of an a-IGZO TFT transducer to contribute to sensitivity amplification. The capacitance ratio (C_{SG}/C_{CG}) increases linearly with the area ratio; therefore, the amplification ratio of the pH sensitivity was easily controlled using the area ratio of SG/CG. The proposed sensor system improved the pH sensitivity by up to 359.28 mV/pH (C_{SG}/C_{CG} = 6.16) at room temperature (300 K), which is significantly larger than the Nernstian limit of 59.14 mV/pH. In addition, the non-ideal behavior, including hysteresis and drift effects, was evaluated to ensure stability and reliability. The amplification of sensitivity based on capacitive coupling was much higher than the increase in the hysteresis voltage and drift rate. Furthermore, we verified the flexibility of the a-IGZO coplanar dual-gate TFT transducer through a bending test, and the electrical properties were maintained without mechanical damage, even after repeated bending. Therefore, the proposed fully transparent and highly sensitive a-IGZO coplanar dual-gate TFT-based pH sensor could be a promising wearable and portable high-performance chemical sensor platform.

Keywords: transparent; flexible; PI substrate; a-IGZO; coplanar dual-gate; capacitive coupling; pH sensor; FET

1. Introduction

Recently, research interest in chemical sensors has increased owing to the increased interest in medical care worldwide, and these sensors can detect signals of small amounts of chemicals or biomolecules. Chemical sensors can be applied to various fields such as food manufacturing, environmental conditioning, and biological monitoring (blood, sweat, urine). Accordingly, many types of chemical sensors for detecting pH, viruses, proteins, and chemicals have been reported [1–3]. Among them, the field-effect transistor (FET)-type sensor platform has attracted considerable interest owing to its excellent features, such as fast response, label-free detection, compatibility with CMOS technology, and easy signal processing [4–6]. In a study by Bergveld, the author considered FET-based sensors as ion-sensitive FETs (ISFETs) [7]. However, because ISFETs detect signals from chemicals through direct contact with the gate dielectric sensing membrane, there is a possibility of its degradation by chemicals. To avoid these reliability-related issues, extended-gate FET (EGFET)-type sensor platforms were introduced [8]. The EGFET consists of two separate parts: a transducer unit and sensing unit. Various high-performance sensing membrane materials have been developed by applying an extended gate that is electrically connected to the gate electrode of the FET to prevent degradation caused by chemical damage [9–11]. However, the most significant limitation hindering the commercialization of

FET-based sensors is the physical sensitivity limit of 59.14 mV/pH at 300 K, which is known as the Nernstian limit [12,13]. Among the many approaches reported in the literature, FET-based sensors with dual-gate structures can overcome the Nernstian limit through the self-amplification of the capacitive coupling between the two gate electrodes [14–18]. Furthermore, interest in portable and wearable sensors as promising next-generation sensor platforms have continued to increase [19–24]. Transparent and flexible sensors can be applied to wearable or portable sensor systems, which results in the point-of care (POC) or real-time monitoring of wound, skin, sweat, and blood that is difficult to achieve with conventional rigid sensor systems. Amorphous oxide semiconductors (AOSs) are widely applied transparent material for transparent TFTs due to their transparency, ease of processing, and high electron mobility [25]. Many studies have been conducted on FET-based sensors fabricated on flexible substrates, including polyimide (PI), polyethylene naphthalate (PEN), and polyethylene terephthalate (PET) [26–30]. In particular, PI is a desirable material for transparent and flexible substrates because it is suitable for CMOS technology owing to its excellent thermal, chemical, and mechanical properties [31,32].

In this study, we propose a fully transparent high-performance coplanar dual-gate thin-film transistor (TFT)-based pH sensor on a flexible PI substrate. We used amorphous indium gallium zinc oxide (a-IGZO) channel layers, indium tin oxide (ITO) source/drain (S/D), and ITO gate electrodes to obtain fully transparent optical properties. An amorphous oxide semiconductor material with high transmittance in the visible light range was used to obtain transparent optical properties [25,33]. We also fabricated an extended gate with an SnO_2 sensing membrane, which ensured excellent sensing properties close to the theoretical Nernstian limit with an acid and base affinity constant of 2.5×10^6 and 1.1×10^{-5}, respectively [18]. Our pH sensor system consists of an a-IGZO coplanar dual-gate TFT transducer and SnO_2 extended-gate (EG) sensing units. In the proposed pH sensor system, we designed a capacitive coupling between the sensing gate (SG) and the control gate (CG) via the floating gate (FG) of the a-IGZO transducer to improve its sensitivity amplification. In particular, the SG and CG were located on the same plane on the gate insulating film, but the FG was located below the a-IGZO FET channel and was electrically separated from the CG and SG by a gate insulating film. The capacitance ratio (C_{SG}/C_{CG}) changes according to the combination of the areas of CG and SG, indicating that the proposed sensor is a self-amplifiable chemical sensor platform with tunable sensitivity. This tunable sensitivity is a beneficial feature of the capacitive coupling-based coplanar dual-gate structure pH sensor that cannot be achieved with a dual-gate structure consisting of a top- and bottom-gate. The C_{SG} and C_{CG} values of top- and bottom-gate structure pH sensors are fixed because they are determined by the pattern size of the channel layer. However, the C_{SG} and C_{CG} values of the proposed coplanar dual-gate structure pH sensors are controlled by the gate electrode pattern sizes because the biases in each gate's electrodes are applied to the channel layer via the FG. Therefore, the proposed coplanar dual-gate pH sensor based on capacitive coupling has the advantage of tunable sensitivity over various conventional chemical sensors. In addition, in comparison to conventional SOI substrate-based dual-gate structure pH sensors, the proposed pH sensor provides various advantages in its material, process, and device design. We also evaluated the non-ideal behavior, such as the hysteresis and drift effects, to ensure its stability and reliability. To ensure its flexibility, the mechanical and electrical stabilities of the a-IGZO coplanar dual-gate TFT transducer on a flexible PI substrate were determined through repeated bending tests.

2. Materials and Methods

Figure 1 shows a schematic illustration of the fabricated a-IGZO coplanar dual-gate TFT transducer and SnO_2 EG sensing units. To construct the pH sensor system, we connected the two units using an electric cable, as indicated by the dotted line. Specifically, the gate electrode of the transducer unit was electrically connected to the conductive layer of the sensing unit to apply the chemical potential of the sensing membrane to the gate electrode. The fully transparent and flexible coplanar dual-gate TFTs were fabricated

to prepare the transducer unit. The transducer unit was fabricated using the following procedure. We prepared 6-µm-thick PI films on 1.5 cm × 1.5 cm size glass plates covered with a 100/100 nm thick SiN_x/SiO_2 adhesive layer. The PI substrates were wet cleaned, for 10 min each, using a standard solvent cleaning process with deionized water (DI) and 2-propyl-alcohol (IPA) in an ultrasonic bath. The substrates were then dried in an oven at 100 °C for 1 h to evaporate the residual solvent and moisture. Subsequently, a 300-nm-thick ITO layer, 100-nm-thick SiO_2 layer, and 50-nm-thick a-IGZO layer were sequentially deposited on the FG, gate insulating film, and channel layer, respectively. The active regions of the TFTs were formed by photolithography and a lift-off process of the a-IGZO layer. The channel width/length ratio of the patterned IGZO channel layer was 80/120 µm. Subsequently, an ITO film with a thickness of 150 nm was deposited, and coplanar dual-gate electrodes (SG, CG) and S/D electrodes were simultaneously formed by a lift-off process. In particular, the CG electrodes patterned with various sizes contributed to achieving various amplification ratios. Finally, the a-IGZO coplanar dual-gate TFT fabricated on the PI substrate was annealed at 250 °C in O_2 ambient for 30 min (PMA). We also prepared the EG sensing unit using the following procedure. A 300-nm-thick ITO conductive layer was deposited as an electrode on a cleaned 1.5 cm × 2.5 cm glass substrate, followed by a 50 nm thick SnO_2 layer as a sensing membrane. Finally, a 0.6 cm inner diameter polydimethylsiloxane (PDMS) reservoir was attached to the SnO_2 sensing membrane to accommodate the electrolyte solution. The ITO, SiO_2, a-IGZO, and SnO_2 layers used for the a-IGZO TFT and SnO_2 EG fabrication were deposited using an RF magnetron sputtering system.
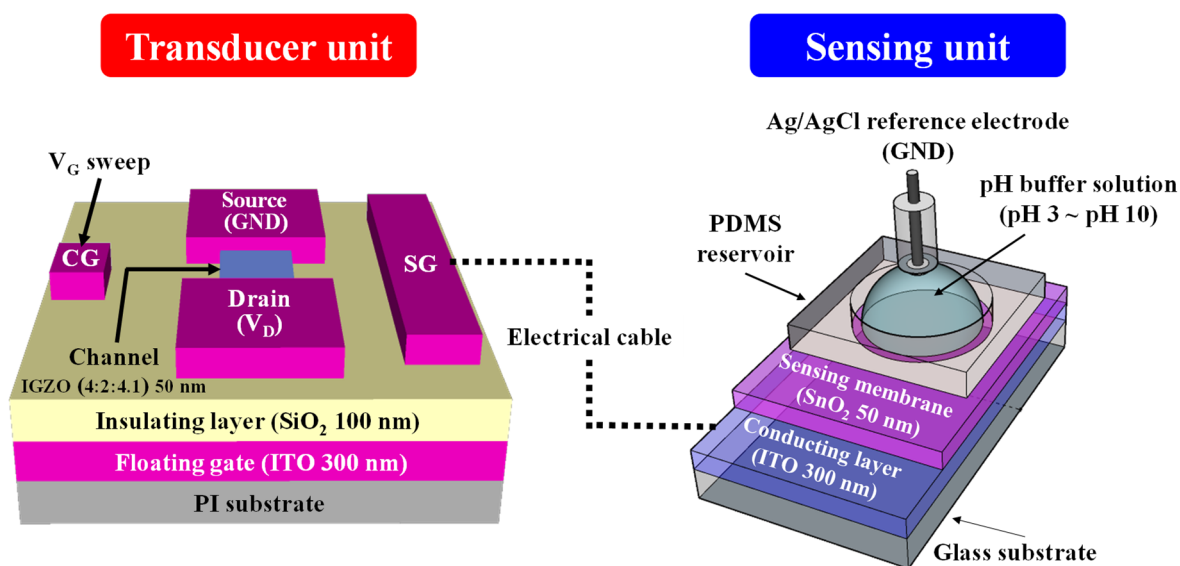

Figure 1. Schematic illustration of an a-IGZO coplanar dual-gate TFT transducer and SnO_2 EG sensing units. The dotted line represents the electrical connection between the two units. Reference electrode is connected to the ground unit of measurement instrument.

Figure 2a,b show photographs of the prepared transparent and flexible a-IGZO coplanar dual-gate TFT transducer and SnO_2 EG sensing units, respectively. Figure 2c shows the optical transmittance spectra of the PI substrate and fabricated a-IGZO coplanar dual-gate TFT transducer unit. The inset shows a photograph of the transparent transducer. The average transmittance of the transducer unit was 76.96% under visible light (wavelength 550–800 nm), whereas that of the PI film was 88.59%.
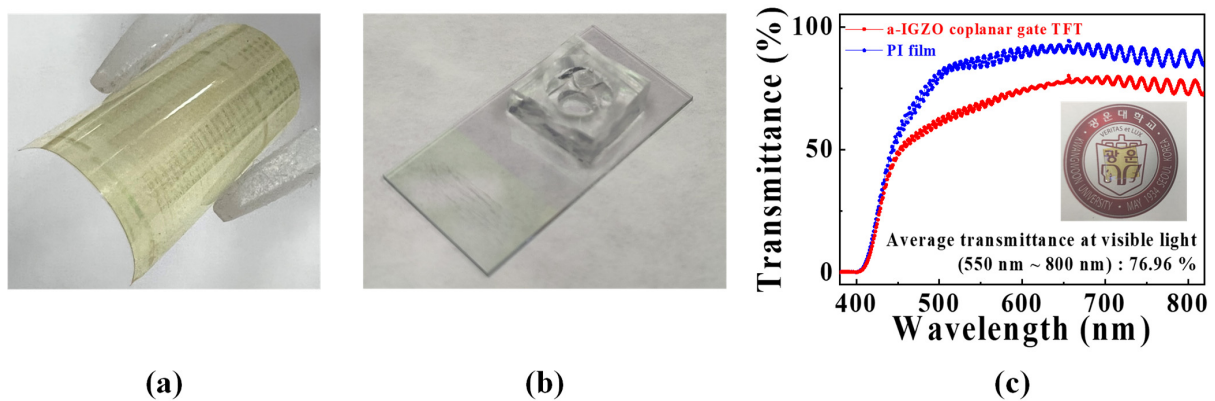
Figure 2. Photographs of the fabricated (**a**) transducer unit and (**b**) sensing unit. (**c**) Optical transmittance spectra of the PI film and a-IGZO coplanar dual-gate TFT transducer unit. The inset shows a photograph of the fabricated transparent transducer unit. The average transmittance at visible light (wavelength 550–800 nm) of the device is 76.96 %.

The capacitance–voltage (C–V) characteristics were measured using an Agilent 4284A Precision LCR meter (Agilent Technologies, Santa Clara, CA, USA). All the electrical characteristics of the a-IGZO TFTs and pH sensor platforms were characterized using an Agilent 4156 B Precision Semiconductor Parameter Analyzer (Agilent Technologies) in a dark box to eliminate noise or light. A pH buffer solution (pH 3.0, 4.0, 6.0, 7.0, 9.0, 10.0) and a commercial Ag/AgCl reference electrode (Horiba 2086A-06T, Kyoto, Japan) were prepared for pH sensing.

3. Results

3.1. C–V Characteristics of the Coplanar Dual-Gate

Figure 3a shows an optical microscope image of a coplanar dual-gate TFT. The SG was designed to have a fixed size of 90×420 µm^2, whereas the CG had various sizes of 90×420 µm^2, 80×200 µm^2, 80×110 µm^2, and 60×70 µm^2. The measured C–V curves for the various CG sizes are shown in Figure 3b. The capacitances of the CGs with the four dimensions specified above were 2.1 pF, 4.54 pF, 6.67 pF, and 12.65 pF, respectively. Meanwhile, the capacitance of the SG was 12.94 pF, which is almost identical to that of the CG of the same size. The relationship between the gate area and capacitance is shown in Figure 3c; the figure shows that the capacitance increased linearly with an increase in the area. The inset shows the relationship between the C_{SG}/C_{CG} and the gate area ratio (A_{SG}/A_{CG}), which indicates that the C_{SG}/C_{CG} is linearly proportional to the A_{SG}/A_{CG}. Therefore, by adjusting the area of the SG and CG, we can easily control the C_{SG}/C_{CG}, which is similar to the amplification ratio in capacitive coupling.
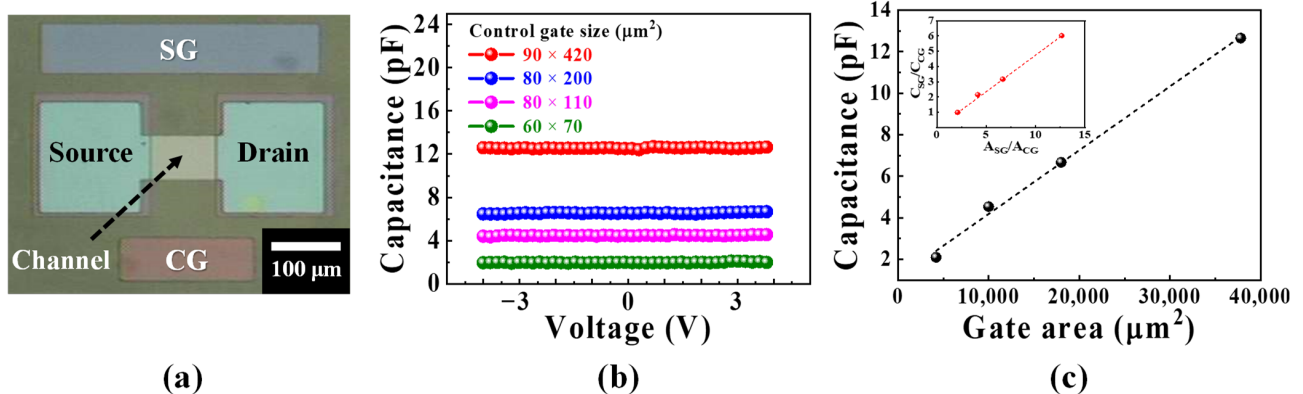

Figure 3. (**a**) Optical microscope image, (**b**) capacitance–voltage curve, and (**c**) capacitance–gate area relationship of the a-IGZO coplanar dual-gate TFT. The inset shows the relationship between C_{SG}/C_{CG} and A_{SG}/A_{CG}.

3.2. DC Bias Coupling Test of the a-IGZO Coplanar Dual-Gate TFT

Figure 4a shows the schematic illustration of the electrical equivalent circuit of an a-IGZO coplanar dual-gate TFT, depicting a simplified model in which the parasitic capacitance components are ignored. The CG where the gate voltage sweeps and the SG where the electrochemical potential of the pH buffer solution is biased are capacitively connected via an electrically isolated FG. In this case, the voltages of the coplanar gates (V_{CG} and V_{SG}) are capacitively coupled to FG (V_{FG}), as expressed in Equation (1). The relationship between V_{CG} and V_{SG} can then be expressed as given in Equation (2). Consequently, the change in the potential of the SG (ΔV_{SG}) can be amplified as the capacitance ratio of the C_{SG}/C_{CG} by capacitive coupling, as expressed in Equation (3). In addition, the ratio of the sensing gate capacitance to the control gate capacitance can modify the relationship between ΔV_{SG} and ΔV_{CG}.

$$V_{FG} = \frac{C_{CG}}{C_{SG} + C_{CG}} V_{CG} + \frac{C_{SG}}{C_{SG} + C_{CG}} V_{SG} \tag{1}$$

$$V_{CG} = \frac{C_{SG} + C_{CG}}{C_{CG}} V_{FG} - \frac{C_{SG}}{C_{CG}} V_{SG} \tag{2}$$

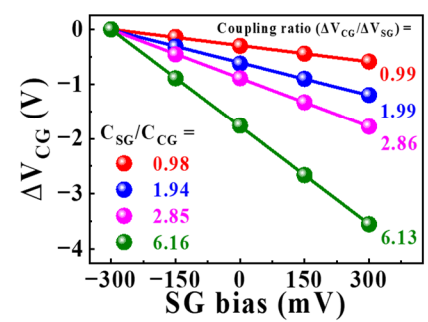$$\therefore \Delta V_{CG} \propto \frac{C_{SG}}{C_{CG}} \Delta V_{SG} \tag{3}$$
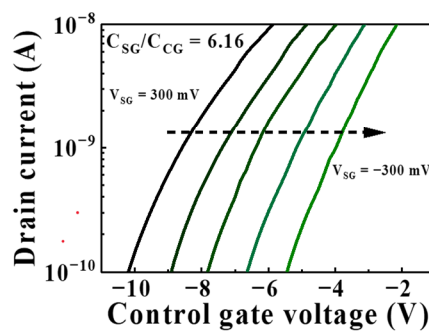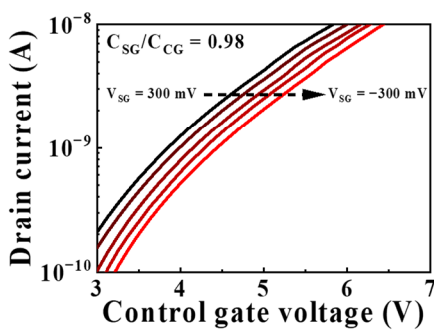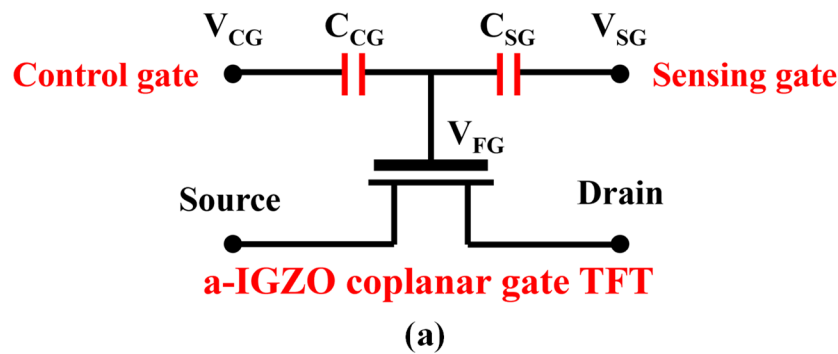

Figure 4. (**a**) Simplified schematic illustration of the electrical equivalent circuit of an a-IGZO coplanar dual-gate TFT. Shifts in the transfer characteristic curve for amplification factor of (**b**) 0.98 and (**c**) 6.16 when SG bias (V_{SG}) is varied from +300 mV to −300 mV at intervals of 150 mV. (**d**) $\Delta V_{CG}/\Delta V_{SG}$ for various values of C_{SG}/C_{CG} obtained at I_{Read} = 1 nA.

Prior to the pH sensing measurements, a DC bias-coupling test was conducted to verify the amplification factor because of capacitive coupling. When a DC bias voltage is applied to the SG, the threshold voltage of the CG shifts according to the magnitude of the SG bias. The shifts in the transfer characteristic curve for C_{SG}/C_{CG} of 0.98 and 6.16 are shown in Figure 4b,c, respectively. When the SG bias was varied between +300 mV and

−300 mV, at intervals of 150 mV, a decrease in the drain current and a rightward shift in the transfer characteristic curve were observed in response to a decrease in the V_{SG}. Figure 4d shows the amplification factor ($\Delta V_{CG}/\Delta V_{SG}$) for various C_{SG}/C_{CG} values extracted at a read drain current (I_{Read}) of 1 nA. It can be observed that there is a linear proportional relationship between $\Delta V_{CG}/\Delta V_{SG}$ and C_{SG}/C_{CG}. For the C_{SG}/C_{CG} values of 0.98, 1.94, 2.85, and 6.16, the values of $\Delta V_{CG}/\Delta V_{SG}$ were 0.99, 1.99, 2.86 and 6.13, respectively. Therefore, we demonstrated that ΔV_{SG} can be amplified by the amplification factor.

Table 1 lists the values of $\Delta V_{CG}/\Delta V_{SG}$ obtained from the DC bias test for various amplification factors.

Table 1. Amplification factors ($\Delta V_{CG}/\Delta V_{SG}$) obtained from the DC bias test of the a-IGZO coplanar dual-gate TFT.

C_{SG}/C_{CG}	$\Delta V_{CG}/\Delta V_{SG}$	R^2 (%)
0.98	0.99	99.93
1.94	1.99	99.95
2.85	2.86	99.99
6.16	6.13	99.98

3.3. pH Sensing Characteristics of the a-IGZO Coplanar Dual-Gate TFT pH sensor

The pH response of the FET-type chemical sensor can be explained by combining the Gouy–Chapman–Stern (GCS) theory and the site-binding model (SBM) [34–36]. According to the GCS theory, an electric double layer is created at the interface between the sensing membrane and the electrolyte solution. In addition, the surface potential (ψ) of the corresponding interface in the SBM is a critical parameter for the ion-sensing capability, which is summarized in Equation (4) [37,38]:

$$2.303\left(pH_{pzc} - pH\right) = \beta\psi + \sinh^{-1}\left[\frac{\sigma_0}{2q(K_b/K_a)^{1/2}N_s}\right] - \ln\left(1 - \frac{\sigma_0}{qN_s}\right) \qquad (4)$$

where k is the Boltzmann constant, T is the temperature of the Kelvin system, q is the elementary charge, β is the dimensionless chemical sensitivity of the sensing membrane, pH_{pzc} is the pH at which the net charge of the surface is zero, σ_0 is the charge density, and the N_s is the total number of the sites per unit area; ψ varies depending on the chemical properties of the sensing membrane and the pH of the electrolyte. The values of the pH_{pzc} and β of SnO_2 that we adopt as sensing membrane are 5.6 and 58.6, respectively. According to this model, the sensing characteristics of the FET-type chemical sensors are determined using $\Delta\psi$. However, in this model, the sensitivity of the conventional single-gate FET-type pH sensor cannot exceed the physical limit of ~59.14 mV/pH at 300 K, which is known as the Nernstian limit. To overcome this fatal drawback, we introduced a coplanar dual-gate structure based on capacitive coupling, which amplifies the small potential change in the SG and makes it detectable in the CG.

Figure 5a,b show the transfer characteristic curves of the a-IGZO coplanar dual-gate TFT pH sensor for C_{SG}/C_{CG} values of 0.98 and 6.16, respectively, indicating that they shift with the pH. The sensing properties were measured with a pH buffer solution of pH 3 to 10 at 300 K. The practical pH sensitivities of various C_{SG}/C_{CG} values obtained at I_{Read} = 1 nA are shown in Figure 5c. The pH sensitivities for C_{SG}/C_{CG} values of 0.98, 1.94, 2.85, and 6.16 were 57.77 mV/pH, 116.4 mV/pH, 174.38 mV/pH, and 359.28 mV/pH, respectively. The pH sensitivity without capacitive coupling (C_{SG}/C_{CG} = 1) was 58.29 mV/pH. It is noteworthy that the proposed sensor exhibited high-performance pH sensing properties that far exceeded the Nernstian limit without additional amplification circuits. This is because the capacitive coupling of the coplanar dual-gate structure enables self-amplification in practical pH sensing operations.
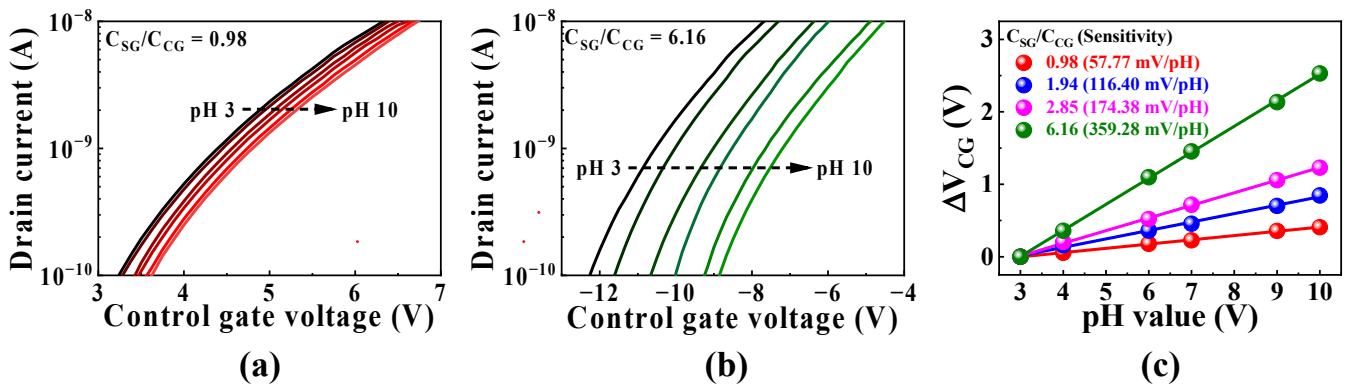
Figure 5. Transfer characteristics curves of the a-IGZO coplanar dual-gate TFT pH sensor in various pH buffer solutions for C_{SG}/C_{CG} of (**a**) 0.98 and (**b**) 6.16. (**c**) pH sensitivity for various C_{SG}/C_{CG} values (I_{Read} = 1 nA).

3.4. Non-Ideal Behavior of the a-IGZO Coplanar Gate TFT pH Sensor

In addition to sensitivity, stability and reliability are important performance indicators of chemical sensors. To verify whether the proposed sensor system ensures repetitive sensing operation over a relatively short period and long period, we measured the hysteresis and drift effects. The hysteresis and drift effects are typical non-ideal behaviors that prevent accurate detection by sensors. The hysteresis effect often arises from the reaction between electrolyte ions (H^+ or OH^-) and the surface, or from the slow transport of ionic species in the sensing membrane bulk [39]. The drift effect is caused by the permeation of ionic species in the electrolyte or by defects in the sensing membrane through hopping or trap-limited transport [40,41]. The hysteresis effect was measured for a total of 50 min by changing the pH of the buffer solution at 300 K in the order of 7→10→7→4→7. Then, the hysteresis voltage (V_H) was extracted from the ΔV_{CG} difference between the start and end points of the pH loop. Figure 6a shows the V_H for various C_{SG}/C_{CG} values; the V_H values were 5.29 mV, 9.13 mV, 13.83 mV, and 20.54 mV for C_{SG}/C_{CG} values of 0.98, 1.94, 2.85, and 6.16, respectively. The drift rate (R_{drift}) was determined by immersion in a pH 7 buffer solution at 300 K for 10 h. Figure 6b shows the drift rates; the R_{drift} values were 7.84 mV/h, 16.71 mV/h, 32.21 mV/h, and 65.08 mV/h for C_{SG}/C_{CG} values of 0.98, 1.94, 2.85 and 6.16, respectively. As capacitive coupling amplifies the surface potential of the sensing membrane connected to the SG, both the V_H and R_{drift} increase with an increase in the C_{SG}/C_{CG}. However, it can be observed that the increments in V_H and R_{drift} are smaller than that of sensitivity.
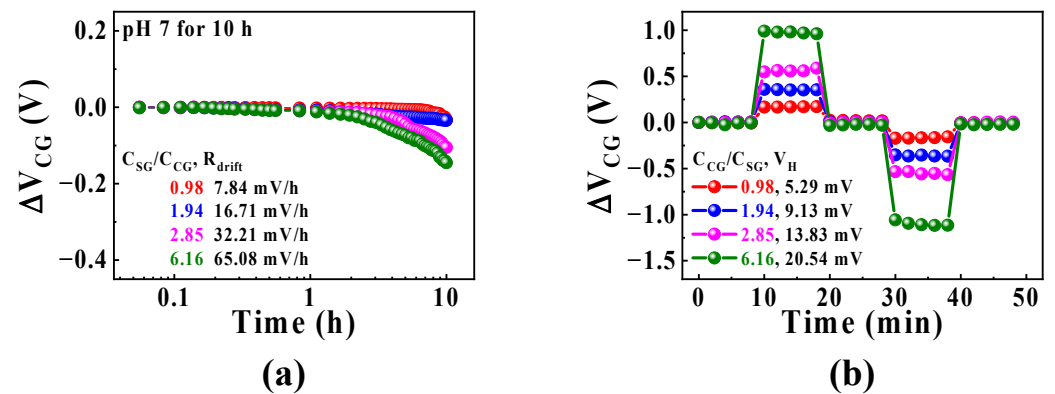

Figure 6. Non-ideal behavior of the a-IGZO coplanar dual-gate TFT pH sensor. (**a**) Hysteresis and (**b**) drift effects for various C_{SG}/C_{CG} values.

Table 2 summarizes the pH sensing properties of the proposed a-IGZO coplanar dual-gate TFT pH sensor. It can be observed that the increments in the V_H and R_{drift} with

an increase in the C_{SG}/C_{CG} are less than 9.1% and 18.5% that of sensitivity, respectively. Therefore, the proposed a-IGZO coplanar gate TFT pH sensor is a stable and reliable chemical sensor platform with a sensitivity high above the Nernstian limit.

Table 2. pH sensing characteristics of the a-IGZO coplanar dual-gate TFT pH sensor.

C_{SG}/C_{CG}	Sensitivity (mV/pH)	$\Delta V_{CG}/\Delta V_{SG}$	V_H (mV)	R_{drift} (mV/h)	V_H to Sensitivity (%)	R_{drift} to Sensitivity (%)
0.98	57.77	0.99	5.29	7.84	9.1	13.3
1.94	116.4	1.99	9.13	16.71	7.8	14.4
2.85	174.38	2.99	13.83	32.21	7.9	18.5
6.16	359.28	6.16	20.54	65.08	5.7	18.1

3.5. Bending Test of the a-IGZO Coplanar Dual Gate TFT

In the sensor system, the flexibility of the sensor must be evaluated by the sensing characteristics after repeated bending operation. For flexible chemical sensor platform applications, it is necessary to maintain the sensing characteristics, including sensitivity and the amplification factor, without a significant degradation of the electrical properties, even after repeated bending operations. As a result of the mechanical stress accompanying the deformation of the flexible PI substrate, various parts of the TFT device, such as the gate insulating film, channels, electrodes, or their interfaces, may undergo irreversible mechanical damage [42].

Figure 7a shows a TFT transducer unit bent to a diameter of 3 mm using a vernier caliper. The inset shows an optical microscope image after the bending test, that is, 500 bending cycles to a diameter of 3 mm. Compared with the sample before the bending test, there were no recognizable defects in the a-IGZO channel, S/D electrode, or coplanar gates, indicating that there was no mechanical damage caused by the bending. Therefore, the bending tests verified the flexibility and mechanical strength of the a-IGZO coplanar dual-gate TFT on the PI substrate. Bending not only affects the optical and mechanical properties, but also the electrical characteristics [42,43]. In FET-type sensor systems in which the electrical characteristics directly affect the sensing characteristics, poor electrical characteristics lead to the deterioration of the sensing characteristics. Therefore, to verify the flexible characteristics of the -IGZO coplanar dual-gate TFT on the PI substrate, we measured the pH sensing characteristics after repeated bending tests. Figure 7b,c show the transfer curves after 500 bending cycles to a diameter of 3 mm for C_{SG}/C_{CG} values of 0.94 and 6.16, respectively. Figure 7d shows the pH sensitivity for various C_{SG}/C_{CG} values after the repeated bending tests. The pH sensitivity obtained from the bending test, using the same samples, slightly decreased from 57.77 mV/pH, 116.4 mV/pH, 174.38 mV/pH, and 359.28 mV/pH before bending to 56.45 mV/pH, 113.6 mV/pH, 165.45 mV/pH, and 345.09 mV/pH after bending, respectively. In addition, slight changes in the $\Delta V_{CG}/\Delta V_{SG}$, from 0.99, 1.99, 2.99, and 6.16 to 0.97, 1.95, 2.84, and 5.92, were observed before and after bending, respectively. It is considered that the slight decrease in the sensitivity and $\Delta V_{CG}/\Delta V_{SG}$ after the bending test is caused by repeated mechanical stresses on the device. However, the decrease in sensitivity is almost negligible, up to 5.1%, and the bent device still gives a high pH sensing performance, above the Nernstian limit, as summarized in Table 3. Accordingly, we conclude that the a-IGZO coplanar dual-gate TFT on a PI substrate is a suitable flexible chemical sensor system that gives a high sensing performance, even after repeated bending tests.
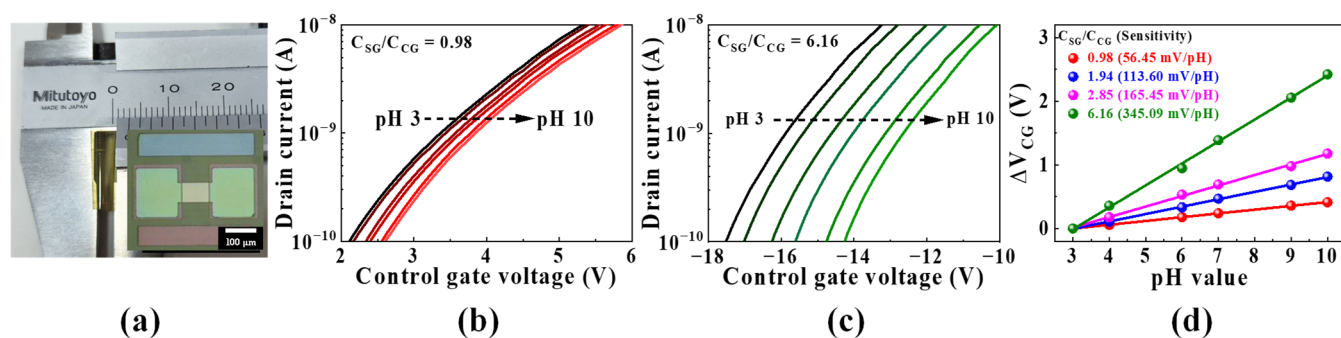
Figure 7. (**a**) Image of an a-IGZO coplanar dual-gate TFT converter unit on a PI substrate bent to a diameter of 3 mm using vernier calipers. The inset shows an optical microscope image obtained after the bending test. Transfer characteristic curves after 500 bending cycles to a diameter of 3 mm for C_{SG}/C_{CG} values of (**b**) 0.98 and (**c**) 6.16. (**d**) pH sensitivity for various C_{SG}/C_{CG} values after repeated bending tests (I_{Read} = 1 nA).

Table 3. PH-sensing characteristics obtained from the bending test of the a-IGZO coplanar dual-gate TFT.

C_{SG}/C_{CG}	Sensitivity before Bending (mV/pH)	Bending Cycles (Times)	Sensitivity after Bending (mV/pH)	Decrease Rate of Sensitivity after Bending (%)
0.98	58.77	100	57.42	2.3
		200	57.28	2.5
		300	56.98	3.0
		400	56.52	3.8
		500	56.45	3.9
1.94	116.40	100	116.08	0.3
		200	115.89	0.4
		300	114.77	1.4
		400	113.73	2.3
		500	113.60	2.4
2.85	174.38	100	173.37	0.6
		200	172.90	0.8
		300	169.46	2.8
		400	168.99	3.1
		500	165.45	5.1
6.16	359.28	100	358.02	0.3
		200	356.69	0.7
		300	351.19	2.3
		400	349.58	2.7
		500	345.09	3.8

4. Conclusions

We investigated a fully transparent and flexible high-performance pH sensor based on an a-IGZO TFT transducer with a coplanar dual-gate structure on a PI substrate. The proposed pH sensor system was constructed by electrically connecting a sensing unit and an a-IGZO TFT transducer unit prepared on different substrates to protect the transducer from chemical damage. The transducer unit consists of an ITO FG, SG electrodes, CG, a-IGZO TFT channel, and ITO S/D electrodes on a flexible PI substrate, which are all transparent materials. The EG sensing unit was prepared on a separate glass substrate. In the proposed pH sensor system, we designed a capacitive coupling between the SG and CG through the FG of the a-IGZO TFT transducer to contribute to sensitivity amplification. We conducted a DC bias-coupling test and found that the C_{SG}/C_{CG} ratio increased linearly with the area ratio of the SG to CG (A_{SG}/A_{CG}) and determined the sensitivity amplification. We measured the potentials of various buffer solutions using a pH sensor composed of an a-IGZO TFT transducer unit and a SnO_2 EG sensing unit and found that the practical

pH sensitivity was amplified in a linear ratio to C_{SG}/C_{CG}. The amplification ratio could be determined by the area ratio of the SG to CG, which increased the pH sensitivity to 359.28 mV/pH at a C_{SG}/C_{CG} value of 6.16; this value is significantly larger than the Nernstian limit of 59.14 mV/pH at room temperature (300 K). In addition, we evaluated the stability and reliability by measuring the non-ideal behaviors, including the hysteresis and drift effects. The amplification of sensitivity with an increase in the C_{SG}/C_{CG} ratio was much larger than the increase in the hysteresis voltage and drift rate, indicating that our proposed a-IGZO coplanar dual-gate TFT pH sensor is a stable and reliable high-sensitivity FET-based chemical sensor platform. Finally, the flexibility of the a-IGZO coplanar dual-gate TFT converter was evaluated via a bending test, and the electrical properties were maintained without mechanical damage, even after 500 bending cycles, to a diameter of 3 mm. Therefore, the fully transparent and highly sensitive IGZO coplanar dual-gate TFT-based pH sensor proposed in this study can be applied to wearable and portable high-performance chemical sensor platforms.

References

1. Singh, A.K.; Pandey, A.; Chakrabarti, P. Fabrication, characterization, and application of CuO nano wires as electrode for ammonia sensing in aqueous environment using extended gate-FET. *IEEE Sens. J.* **2021**, *21*, 5779–5786. [CrossRef]
2. Capua, L.; Sprunger, Y.; Elettro, H.; Risch, F.; Grammoustianou, A.; Midahuen, R.; Ernst, T.; Barraud, S.; Gill, R.; Ionescu, A.M. Label-free C-reactive protein Si nanowire FET sensor arrays with super-Nernstian back-gate operation. *IEEE Trans. Electron Devices* **2022**, *69*, 2159–2165. [CrossRef]
3. Dolai, S.; Tabib-Azar, M. Zika virus field effect transistor. *IEEE Sens. J.* **2021**, *21*, 4122–4128. [CrossRef]
4. Bausells, J.; Carrabina, J.; Errachid, A.; Merlos, A. Ion-sensitive field-effect transistors fabricated in a commercial CMOS technology. *Sens. Actuators B Chem.* **1999**, *57*, 56–62. [CrossRef]
5. Moser, N.; Lande, T.S.; Toumazou, C.; Georgiou, P. ISFETs in CMOS and emergent trends in instrumentation: A review. *IEEE Sens. J.* **2016**, *16*, 6496–6514. [CrossRef]
6. Olthuis, W.; Robben, M.A.M.; Bergveld, P.; Bos, M.; van der Linden, W.E. pH sensor properties of electrochemically grown iridium oxide. *Sens. Actuators B Chem.* **1990**, *2*, 247–256. [CrossRef]
7. Bergveld, P. Development of an ion-sensitive solid-state device for neurophysiological measurements. *IEEE Trans. Biomed. Eng.* **1970**, *BME-17*, 70–71. [CrossRef]
8. van der Spiegel, J.; Lauks, I.; Chan, P.; Babic, D. The extended gate chemically sensitive field effect transistor as multi-species microprobe. *Sens. Actuators* **1983**, *4*, 291–298. [CrossRef]
9. Rao, L.; Wang, P.; Qian, Y.; Zhou, G.; Nötzel, R. Comparison of the extended gate field-effect transistor with direct potentiometric sensing for super-Nernstian InN/InGaN quantum dots. *ACS Omega* **2020**, *5*, 32800–32805. [CrossRef] [PubMed]
10. Xue, M.; Mackin, C.; Weng, W.-H.; Zhu, J.; Luo, Y.; Luo, S.-X.L.; Lu, A.-Y.; Hempel, M.; McVay, E.; Kong, J.; et al. Integrated biosensor platform based on graphene transistor arrays for real-time high-accuracy ion sensing. *Nat. Commun.* **2022**, *13*, 5064. [CrossRef]
11. Chen, C.-P.; Ganguly, A.; Lu, C.-Y.; Chen, T.-Y.; Kuo, C.-C.; Chen, R.-S.; Tu, W.-H.; Fischer, W.B.; Chen, K.-H.; Chen, L.-C. Ultrasensitive in situ label-free DNA detection using a GaN nanowire-based extended-gate field-effect-transistor sensor. *Anal. Chem.* **2011**, *83*, 1938–1943. [CrossRef]

12. Spijkman, M.; Smits, E.C.P.; Cillessen, J.F.M.; Biscarini, F.; Blom, P.W.M.; de Leeuw, D.M. Beyond the Nernst-limit with dual-gate ZnO ion-sensitive field-effect transistors. *Appl. Phys. Lett.* **2011**, *98*, 043502. [CrossRef]

13. Knopfmacher, O.; Tarasov, A.; Fu, W.; Wipf, M.; Niesen, B.; Calame, M.; Schönenberger, C. Nernst limit in dual-gated Si-nanowire FET sensors. *Nano Lett.* **2010**, *10*, 2268–2274. [CrossRef]

14. Spijkman, M.-J.; Myny, K.; Smits, E.C.P.; Heremans, P.; Blom, P.W.M.; de Leeuw, D.M. Dual-gate thin-film transistors, integrated circuits and sensors. *Adv. Mater.* **2011**, *23*, 3231–3242. [CrossRef] [PubMed]

15. Lee, I.-K.; Lee, K.H.; Lee, S.; Cho, W.-J. Microwave annealing effect for highly reliable biosensor: Dual-gate ion-sensitive field-effect transistor using amorphous InGaZnO thin-film transistor. *ACS Appl. Mater. Interfaces* **2014**, *6*, 22680–22686. [CrossRef] [PubMed]

16. Cheng, Q.; Wang, M.; Tao, M.; Yin, R.; Li, Y.; Yang, N.; Xu, W.; Gao, C.; Hao, Y.; Yang, Z. Planar dual gate GaN HEMT cascode amplifier as a voltage readout PH sensor with high and tunable sensitivities. *IEEE Electron Device Lett.* **2020**, *41*, 485–488. [CrossRef]

17. Jang, H.-J.; Gu, J.-G.; Cho, W.-J. Sensitivity enhancement of amorphous InGaZnO thin film transistor based extended gate field-effect transistors with dual-gate operation. *Sens. Actuators B Chem.* **2013**, *181*, 880–884. [CrossRef]

18. Cho, S.-K.; Cho, W.-J. Ultra-high sensitivity pH-sensors using silicon nanowire channel dual-gate field-effect transistors fabricated by electrospun polyvinylpyrrolidone nanofibers pattern template transfer. *Sens. Actuators B Chem.* **2021**, *326*, 128835. [CrossRef]

19. Costa, J.C.; Pouryazdan, A.; Panidi, J.; Spina, F.; Anthopoulos, T.D.; Liedke, M.O.; Schneider, C.; Wagner, A.; Münzenrieder, N. Flexible IGZO TFTs and their suitability for space applications. *IEEE J. Electron Devices Soc.* **2019**, *7*, 1182–1190. [CrossRef]

20. Segev-Bar, M.; Haick, H. Flexible sensors based on nanoparticles. *ACS Nano* **2013**, *7*, 8366–8378. [CrossRef]

21. Hu, B.; Chen, W.; Zhou, J. High performance flexible sensor based on inorganic nanomaterials. *Sens. Actuators B Chem.* **2013**, *176*, 522–533. [CrossRef]

22. Xu, K.; Lu, Y.; Takei, K. Multifunctional skin-inspired flexible sensor systems for wearable electronics. *Adv. Mater. Technol.* **2019**, *4*, 1800628. [CrossRef]

23. Nag, A.; Mukhopadhyay, S.C.; Kosel, J. Wearable flexible Sensors: A review. *IEEE Sens. J.* **2017**, *17*, 3949–3960. [CrossRef]

24. Nakata, S.; Arie, T.; Akita, S.; Takei, K. Wearable, flexible, and multifunctional healthcare device with an ISFET chemical sensor for simultaneous sweat PH and skin temperature monitoring. *ACS Sens.* **2017**, *2*, 443–448. [CrossRef]

25. Kamiya, T.; Hosono, H. Material characteristics can applications of transparent amorphous oxide semiconductor. *NPG Asia Mater.* **2010**, *2*, 15–22. [CrossRef]

26. Han, S.-T.; Peng, H.; Sun, Q.; Venkatesh, S.; Chung, K.-S.; Lau, S.C.; Zhou, Y.; Roy, V.A.L. An overview of the development of flexible sensors. *Adv. Mater.* **2017**, *29*, 1700375. [CrossRef]

27. Vilela, D.; Romeo, A.; Sánchez, S. Flexible sensors for biomedical technology. *Lab A Chip* **2016**, *16*, 402–408. [CrossRef]

28. Jakob, M.H.; Gutsch, S.; Chatelle, C.; Krishnaraja, A.; Fahlteich, J.; Weber, W.; Zacharias, M. Flexible thin film PH sensor based on low-temperature atomic layer deposition. *Phys. Status Solidi-Rapid Res. Lett.* **2017**, *11*, 1700123. [CrossRef]

29. Mansouri Majd, S.; Salimi, A. Ultrasensitive flexible FET-type aptasensor for CA 125 cancer marker detection based on carboxylated multiwalled carbon nanotubes immobilized onto reduced graphene oxide film. *Anal. Chim. Acta* **2018**, *1000*, 273–282. [CrossRef]

30. Park, S.J.; Kwon, O.S.; Lee, S.H.; Song, H.S.; Park, T.H.; Jang, J. Ultrasensitive flexible graphene based field-effect transistor (FET)-type bioelectronic nose. *Nano Lett.* **2012**, *12*, 5082–5090. [CrossRef]

31. Singh, K.; Her, J.-L.; Lou, B.-S.; Pang, S.-T.; Pan, T.-M. An extended-gate FET-based pH sensor with an InZnxOy membrane fabricated on a flexible polyimide substrate at room temperature. *IEEE Electron Device Lett.* **2019**, *40*, 804–807. [CrossRef]

32. Gao, X.; Lin, L.; Liu, Y.; Huang, X. LTPS TFT process on polyimide substrate for flexible AMOLED. *J. Disp. Technol.* **2015**, *11*, 666–669. [CrossRef]

33. Kamiya, T.; Nomura, K.; Hosono, H. Present status of amorphous In–Ga–Zn–O thin-film transistors. *Sci. Technol. Adv. Mater.* **2010**, *11*, 044305. [CrossRef]

34. Chen, S.; Bomer, J.G.; Carlen, E.T.; van den Berg, A. Al2O3/silicon nanoISFET with near ideal Nernstian response. *Nano Lett.* **2011**, *11*, 2334–2341. [CrossRef]

35. Yates, D.E.; Levine, S.; Healy, T.W. Site-binding model of the electrical double layer at the oxide/water interface. *J. Chem. Soc. Faraday Trans. 1* **1974**, *70*, 1807–1818. [CrossRef]

36. Tarasov, A.; Wipf, M.; Bedner, K.; Kurz, J.; Fu, W.; Guzenko, V.A.; Knopfmacher, O.; Stoop, R.L.; Calame, M.; Schönenberger, C. True reference nanosensor realized with silicon nanowires. *Langmuir* **2012**, *28*, 9899–9905. [CrossRef] [PubMed]

37. Landheer, D.; Aers, G.; McKinnon, W.R.; Deen, M.J.; Ranuares, J.C. Model for the field effect from layers of biological macromolecules on the gates of metal-oxide semiconductor transistors. *J. Appl. Phys* **2005**, *98*, 044701. [CrossRef]

38. Chou, J.-C.; Liao, L.P. Study on pH at the point of zero charge of TiO2 pH ion-sensitive field effect transistor made by the sputtering method. *Thin Solid Film.* **2005**, *476*, 157–161. [CrossRef]

39. Tsai, C.-N.; Chou, J.-C.; Sun, T.-P.; Hsiung, S.-K. Study on the sensing characteristics and hysteresis effect of the tin oxide pH electrode. *Sens. Actuators B Chem* **2005**, *108*, 877–882. [CrossRef]

40. Jamasb, S.; Collins, S.; Smith, R.L. A physical model for drift in pH ISFETs. *Sens. Actuators B Chem.* **1998**, *49*, 146–155. [CrossRef]

41. Bousse, L.; Bergveld, P. The role of buried OH sites in the response mechanism of inorganic-gate pH-sensitive ISFETs. *Sens. Actuators* **1984**, *6*, 65–78. [CrossRef]

42. Cheng, J.; Wu, L.; Du, X.-W.; Jin, Q.-H.; Zhao, J.-L.; Xu, Y.-S. Flexible solution-gated graphene field effect transistor for electrophysiological recording. *J. Microelectromech Syst.* **2014**, *23*, 1311–1317. [CrossRef]
43. Shin, K.; Xiong, W.; Cho, C.Y.; Cleavelin, C.R.; Schulz, T.; Schruefer, K.; Patruno, P.; Smith, L.; Liu, T.-J.K. Study of bending-induced strain effects on MuGFET performance. *IEEE Electron Device Lett.* **2006**, *27*, 671–673. [CrossRef]